Readout fidelity of coaxial holographic digital data page recording in nanoparticle (thiol ene) polymer composites

doi: 10.7567/JJAP.55.09SB03

Readout Fidelity of Coaxial Holographic Digital Data Page Recording in Nanoparticle-(Thiol-Ene) Polymer Composites

Kohta Nagaya, Eiji Hata and Yasuo Tomita*

Department of Engineering Science, University of Electro-Communications, 1-5-1 Chofugaoka, Chofu, Tokyo 182-8585, Japan

We report on an experimental investigation of nanoparticle-concentration and thiol-to-ene stoichiometric ratio dependences of symbol error rates (SERs) and signal-to-noise ratios (SNRs) of digital data pages recorded at a wavelength of 532 nm in thiol-ene based nanoparticle-polymer composite (NPC) films by using a coaxial holographic digital data storage method. We show that SERs and SNRs at the optimized material condition can be lower than 1×10^{-4} and higher than 10, respectively, without error correction coding. These results show the usefulness of thiol-ene based NPCs as coaxial holographic data storage media.

1. Introduction

Holographic photopolymers have been extensively investigated for their use in photonics and information display.[1–3] In particular, various photopolymer materials have been studied for holographic data storage (HDS) systems that generally require saturated refractive index modulation amplitudes (Δn_{sat}) larger than 5×10^{-3}, material recording sensitivities (S) higher than 500 cm/J at visible recording wavelengths, polymerization shrinkage lower than 0.5% and high thermal stability.[4] These recording materials may be categorized into all-organic photopolymers[2,5] and inorganic-organic multicomponent photopolymers, the so-called photopolymerizable nanoparticle-polymer composites (NPCs).[6–11] It has been shown that NPCs using thiol-ene monomer capable of radical mediated step-growth polymerizations can satisfy all the above demanding requirements for HDS recording media.[12,13] This is so because holographically assembled nanoparticles[14] provide Δn_{sat} as large as 1×10^{-2} and shrinkage suppression lower than 0.5% as well as forming rigid nanocomposite structures with increased glass transition temperature.[13,15] Subsequently, such thiol-ene based NPCs were used to demonstrate hologram shift-multiplexing of digital data storage more than 200 pages with high fidelity in two-

*E-mail address: ytomita@uec.ac.jp

beam holography setup.[16,17] In this paper we demonstrate coaxial holographic digital data page recording[18,19] in thiol-ene based NPCs at a wavelength of 532 nm. We investigate nanoparticle-concentration and thiol-to-ene stoichiometric ratio dependences of readout fidelity of stored digital data pages.

2. Sample preparation using thiol-ene formulation

Step-growth (thiol-ene) polymerizations are based on the radical addition of a thiol to a vinyl functional group with the final product resulting from a combination of the thiol and ene functional groups.[20] Their polymerization proceeds by a step-growth addition mechanism via sequential propagation of a thiyl radical through a vinyl functional group and the subsequent chain transfer to the thiol, regenerating the thiyl radical. Because the molecular weight increases throughout the course of the reaction and high-molecular-weight polymer is not obtained until the end of the polymerization, gelation occurs late in conversion during reaction. Therefore, bulk polymerization shrinkage occurring before the gelation can be readily accommodated by the liquid mixture of oligomers as compared with radical mediated chain-growth polymerization of crosslinking (meth)acrylate monomer.[21]

We employed such thiol-ene formulation that consisted of a secondary thiol monomer [1,4-bis(3-mercaptobutyryloxy) butane (dithiol, Showa Denko K.K.)] with high shelf-life stability and low odor, and an allyl triazine triene monomer [triallyl-1,3,5-triazine-2,4,6(1H,3H,5H)-trione (TATATO, Aldrich)] with rigid structure and high electron density. We mixed the thiol-ene monomer at various ratios of the thiol-to-ene stoichiometry (r) with silica nanoparticles (the average size of 13 nm) dissolved in methyl isobutyl ketone to make stoichiometric and nonstoichiometric thiol-ene based NPCs. In order to sensitize them in the green, we employed a titanocene organo-metallic complex (Irgacure 784, Ciba), in combination with benzoyl peroxide (BzO_2, Aldrich), as a visible initiator/sensitizer system.[22] For efficient step-growth thiol-ene polymerization we employed Irgacure 784 of 2 wt.% and BzO_2 of 2.5 wt.% with respect to the thiol-ene monomer blend. Chemical structures of these thiol-ene formulation are shown in Fig. 1. This thiol-ene based NPC mixture was cast on a spacer-loaded glass plate and was covered with another glass plate after drying procedure to make thiol-ene based NPC film samples for our holographic recording measurements.

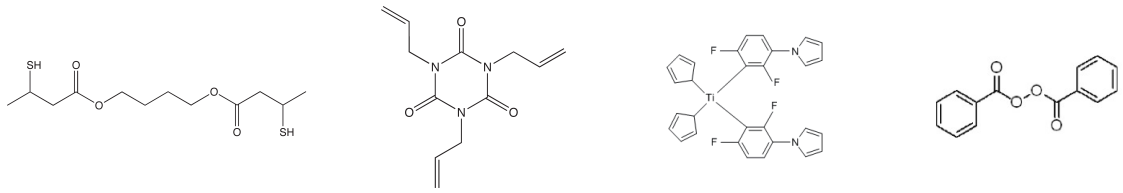

(a) (b) (c) (d)

Fig. 1. Chemical structures of (a) dithiol, (b) TATATO, (c) Irgacure 784 and (d) BzO_2.

3. Effect of nanoparticle concentration and thiol-ene stoichiometry ratio on plane-wave volume holograms

It has been shown that thiol-ene based NPCs have strong dependences of $\Delta n_{\rm sat}$ and polymerization shrinkage on r.[13,23] In order to compare these dependences for plane-wave volume holograms with those of readout fidelity of coaxial holographic digital data page recording in this paper, we briefly describe the former results. In the measurement we used a two-beam interference setup to record an unslanted transmission plane-wave volume hologram of 1-μm spacing with two mutually coherent beams of equal intensities from a cw Nd:YVO_4 laser (Verdi, Coherent Inc.) operating at 532 nm. The diffraction efficiency from a volume hologram being recorded in a thiol-ene based NPC film sample with 10-μm spacer was monitored in real time by a low intensity and photo-insensitive He-Ne laser beam at 633 nm. All the beams were s polarized. We extracted $\Delta n_{\rm sat}$ from the saturated diffraction efficiency and the effective thickness that was estimated from Bragg-angle detuning data.[13] Figure 2(a) shows nanoparticle-concentration dependences of $\Delta n_{\rm sat}$ and the out-of-plane fractional thickness change (σ) due to shrinkage for plane-wave NPC volume holograms recorded at the stoichiometric composition (r=1).[13] It can be seen that $\Delta n_{\rm sat}$ is maximized close to 1×10^{-2} and σ is as low as 0.5 % at 25 vol.% silica nanoparticle concentration, meeting the requirements of HDS media.[4] Similar trends of $\Delta n_{\rm sat}$ and σ as a function of silica nanoparticle concentration were reported for other NPCs.[6–11] Figure 2(b) shows $\Delta n_{\rm sat}$ and σ as a function of r for NPC volume gratings at 25 vol.% silica nanoparticle concentration.[23] It can be seen that while $\Delta n_{\rm sat}$ is maximized at r=1, σ decreases below 0.5 % as thiol becomes excessive (*i.e.*, $r > 1$). We attribute the trend of $\Delta n_{\rm sat}$ to the fact that while the stoichiometric composition gives the highest polymerization rate, unreacted excess monomer is left in non-stoichiometric thiol-ene based NPC films.[23] The increasing trend

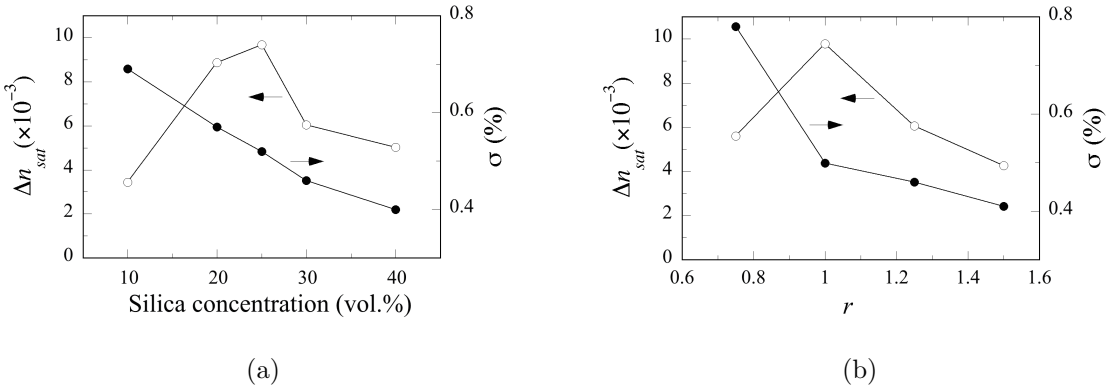

Fig. 2. (a) Nanoparticle-concentration dependences of Δn_{sat} (○) and σ (●) on silica nanoparticle concentration at $r = 1$. (b) Dependences of Δn_{sat} (○) and σ (●) on r at 25 vol.% silica nanoparticle concentration.

of σ with decreasing r can be explained by the homopolymerization of TATATO.[23)]

4. Coaxial holographic digital data page recording

Figure 3 shows our optical setup for coaxial holographic digital data recording in thiolene based NPC films. The linearly polarized laser beam from a cw Nd:YVO_4 laser operating at 532 nm was used for both recording and readout. The expanded and collimated laser beam was normally incident on a transmission-type liquid crystal spatial light modulator (LC2002, HOLOEYE Photonics AG) with 1024×768 pixels and a pixel pitch of 36 μm. A computer-generated circular and concentric input page pattern

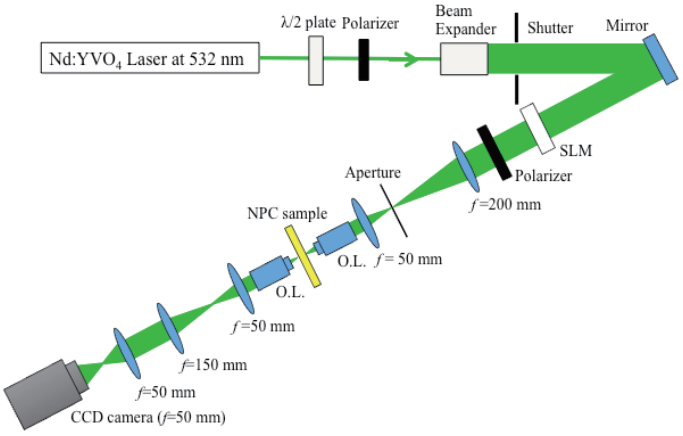

Fig. 3. Optical setup for coaxial holographic digital data page recording. SLM: spatial light modulator; O.L.: objective lens.

for digital signal and reference data, respectively, was encoded on the incident collimated beam via the spatial light modulator. We employed the 9:16 modulation coding format[24] (see Fig. 4a) to encode two-dimensional digital data page information with randomly generated balanced-binary data bits (*i.e.*, an equal number of 0s and 1s), together with randomly generated balanced-binary reference bits (see Fig. 4b). This is so because the coding format gave the lowest symbol error rate (SER) and the highest signal-to-noise ratio (SNR) among other coding formats in two-beam shift-multiplexing holographic recording.[17] The transmitted data-bearing beam was loosely focused on a thiol-ene based NPC film sample of $\sim$100 μm thickness via two relay lenses and an objective lens (NA=0.55) for volume holographic recording. The position of the thiol-ene based NPC film sample was approximately 200 μm away from the focus point. The recording was done at an input intensity of 11 mW/cm^2 for 20 s after 25-second uniform pre-exposure followed by uniform post-exposure by a low coherence light-emitting diode (LED) operating at 532 nm in order to avoid holographic scattering that takes place for thick photosensitive materials with large refractive index changes.[25,26] The reconstructed digital data page was readout by a beam with the corresponding reference pattern and was imaged onto an 3296$\times$2472 CCD camera (ARTCAM-810KAI-USB3, ARTRAY) with 5.5 μm pixels at an oversampling rate of 6 via a tandem combination of an objective lens (NA=0.55) and two relay lenses.

(a) (b)

Fig. 4. (a) 9:16 symbol modulation code pattern. (b) Input digital data page with coded signal and reference patterns.

A magnified input digital data page with the 9:16 symbol modulation code and its reconstructed straight-through image through a uniformly cured thiol-ene NPC film sample by the LED and the optics of the object arm are illustrated in Figs. 5(a) and 5(b), respectively. In Fig. 5(a) one data page displayed on an SLM consists of the

(a) (b)

Fig. 5. (a) Input digital data page with the 9:16 symbol modulation code, (b) straight-through image with a uniformly cured thiol-ene based NPC film sample of ∼100-μm thickness.

data size of 12969 bits that correspond to 14441 symbol data of information. It was found that an SER and an SNR of the straight-through image were 7.7×10^{-5} and 14, respectively. It is known that error-free retrieval of data pages with an SER of lower than 1×10^{-1} is possible with error correction code (ECC).[19,27] Therefore, the baseline performance of the optical system is sufficient to evaluate the holographic data page recording capability of thiol-ene based NPCs.

Figure 6 shows SERs and SNRs of reconstructed data pages at silica nanoparticle concentrations of 15 vol.% (Fig. 6a), 25 vol.% (Fig. 6b) and 35 vol.% (Fig. 6c) when the thiol-ene stoichiometric composition (r =1) was used. It was found that the corresponding SERs (SNRs) were 1.5×10^{-3} (4.3), 7.7×10^{-5} (12) and 1.3×10^{-4} (4.8) at silica nanoparticle concentrations of 15 vol.%, 25 vol.% and 35 vol.%, respectively. Silica nanoparticle-concentration dependences of SERs and SNRs at $r = 1$ are summarized in Fig. 7. It can be seen that SERs (SNRs) are minimized (maximized) at 25 vol.% silica nanoparticle concentration, where Δn_{sat} is maximized as shown in Fig. 2a. It can

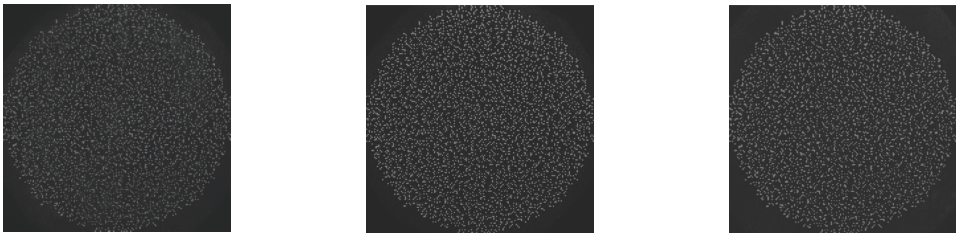

(a) (b) (c)

Fig. 6. Reconstructed digital data pages from holograms recorded in thiol-ene based stoichiometric NPCs at silica nanoparticle concentrations of (a) 15 vol.%, (b) 25 vol.% and (c) 35 vol.%.

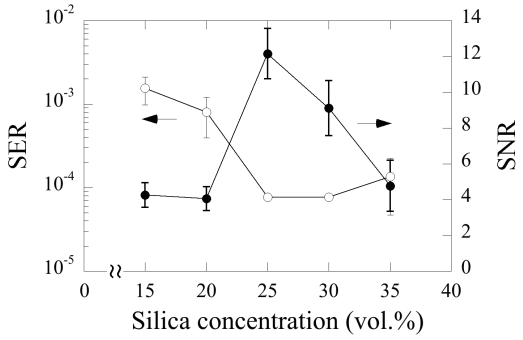

Fig. 7. Silica nanoparticle-concentration dependences of SERs (○) and SNRs (●) at $r = 1$.

also be seen that SERs rapidly increase at silica nanoparticle concentrations lower than 25 vol.% due to decreased (increased) Δn_{sat} (σ). It is found that while SNRs rapidly decrease with increasing silica nanoparticle concentrations higher than 25 vol.%, SERs are rather insensitive to an increase in silica nanoparticle concentrations. These trends may be explained by the following reasons: while SNRs are susceptible with increased light scattering noise at high concentrations of silica nanoparticles, an increase in SER by increased light scattering noise is compensated for by the suppression of σ with increasing silica nanoparticle concentrations.

Figure 8 shows thiol-ene strochiometric ratio dependences of SERs and SNRs of reconstructed data pages at $r = 0.75$ (Fig. 8a), 1.00 (Fig. 8b) and 1.50 (Fig. 8c) when silica nanoparticle concentration of 25 vol.% was used. It was found that the corresponding SERs (SNRs) were 7.8×10^{-5} (10), 7.7×10^{-5} (13) and 1.0×10^{-4} (6) at $r = 0.75$, 1.00 and 1.50, respectively. Thiol-ene stoichiometric ratio dependences of SERs and SNRs at 25 vol.% silica nanoparticles are summarized in Fig. 9. It can be seen that the best

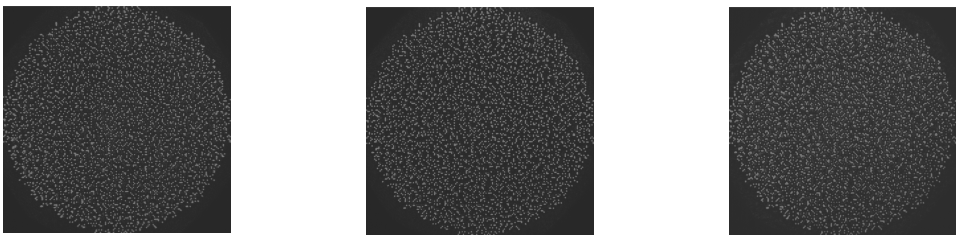

(a) (b) (c)

Fig. 8. Reconstructed digital data pages from holograms recorded in thiol-ene based NPCs at $r =$ (a) 0.75, (b) 1.00 and (c) 1.50 and at 25 vol.% silica nanoparticles.

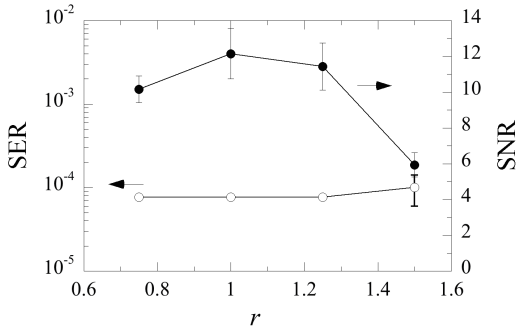

Fig. 9. Thiol-ene stoichiometric ratio dependences of SERs (○) and SNRs (●) at 25 vol.% silica nanopartcle concentration.

fidelity is obtained at r=1, where $\Delta n_{\rm sat}$ is maximized and σ is approximately 0.5 % as shown in Fig. 2b. It is interesting to note that while SNRs exibit a weak dependence on r, SERs substantively shows no dependence of r. The latter unexpected result requires further investigations.

Finally, we would like to comment on an influence of the spatial frequency response of a recorded NPC transmission grating on the readout fidelity in our coaxial holographic digital data page recording system. We showed that values for $\Delta n_{\rm sat}$ of plane-wave transmission gratings recorded in thiol-ene based NPCs were more or less 1×10^{-2} or larger at grating spacing between 0.4 and 1.4 μm but they rapidly decreased at grating spacing shorter than 0.4 μm.[13] The cut-off spatial frequency of our coaxial recording system is of the order of NA/λ, which approximately corresponds to the spatial frequency of a 1-μm grating for NA=0.55 and at λ=532 nm. It is comparable to the case of our two-beam holography setup where the incident angle between object and reference beams was 30.9°.[16,17] Therefore, we consider that the spatial frequency dependence of a thiol-ene based NPC transmission grating does not cause any negative effect on the readout fidelity in our two-beam holography and coaxial recording setup.

5. Conclusion

We have studied nanoparticle-concentration and thiol-ene stoichiometric ratio dependences of SER and SNR of digital data pages recorded in thiol-ene based NPCs at a wavelength of 532 nm by using a coaxial holographic digital data storage method. We have found that measured SERs and SNRs are minimized and maximized, respectively, at 25 vol.% silica nanoparticle concentration and r =1 that maximize $\Delta n_{\rm sat}$ of a plane-wave volume grating. SERs and SNRs under these optimum material condition

are lower than 1×10^{-4} and higher than 10, respectively, without ECC, indicating possible error-free retrieval of digital data pages with ECC. We have also found that SERs are weakly dependent on σ within the range below 0.8 % at varied silica nanoparticle concentrations and r. Our results show the usefulness of thiol-ene based NPCs as HDS media in a coaxial holographic recording system that provides high storage capacity. Our study of the hologram shift-multiplexing capability of thiol-ene NPCs in a coaxial holographic recording system with improved recording schemes[28–30] is underway.

Acknowledgment

This work was supported by the Ministry of Education, Culture, Sports, Science and Technology of Japan under grant 15H03576.

References

1) R.A. Lessard and G. Manivannan, Proc. SPIE **2405**, 2 (1995).
2) K. Curtis, L. Dhar, A. Hill, W. Wilson, and M. Ayres eds., *Holographic Data Storage: From Theory to Practical Systems* (Wiley, Hoboken, 2010).
3) H. Horimai, Proc. International Workshop on Holography and Related Technologies 2015 (IWH 2015), Tu2-4 (2015).
4) L. Dhar, M. G. Schnoes, H. E. Katz, A. Hale, M. L. Schilling, and A. L. Harris, "Photopolymers for digital holographic data storage," in *Holographic Data Storage*, H. J. Coufal, D. Psaltis, and G. T. Sincerbox, eds. (Springer, Berlin, 2000), pp. 199.
5) R. T. Ingwall and D. Waldman, "Photopolymer systems," in *Holographic Data Storage*, H. J. Coufal, D. Psaltis, and G. T. Sincerbox, eds. (Springer, Berlin, 2000), pp. 171.
6) N. Suzuki, Y. Tomita, and T. Kojima, Appl. Phys. Lett. **81**, 4121 (2002).
7) N. Suzuki and Y. Tomita, Appl. Opt. **43**, 2125 (2004).
8) N. Suzuki, Y. Tomita, K. Ohmori, M. Hidaka, and K. Chikama, Opt. Express **14**, 12712 (2006).
9) Y. Tomita, "Holographic Nanoparticle-photopolymer composites," in H.S. Nalwa ed., *Encyclopedia of Nanoscience and Nanotechnology* **15** (American Scientific Publishers, Valencia, 2011), p. 191.
10) R. Fujii, J. Guo, J. Klepp, C. Pruner, M. Fally, and Y. Tomita, Opt. Lett. **39**, 3453 (2014).
11) Y. Tomita, E. Hata, K. Momose, K. Chikama, C. Pruner, J. Klepp, and M. Fally, J. Mod. Opt. **63**, S11 (2016).
12) E. Hata and Y. Tomita, Opt. Lett. **35**, 396 (2010).
13) E. Hata, K. Mitsube, K. Momose, and Y. Tomita, Opt. Mater. Express **1**, 207 (2011).
14) Y. Tomita, N. Suzuki, and K. Chikama, Opt. Lett. **30**, 839 (2005).
15) Y. Tomita, T. Nakamura, and A. Tago, Opt. Lett. **33**, 1750 (2008).
16) K. Momose, S. Takayama, E. Hata, and Y. Tomita, Opt. Lett. **37**, 2250 (2012).
17) S. Takayama, K. Nagaya, K. Momose, and Y. Tomita, Appl. Opt. **53**, B53 (2014).
18) H. Horimai, X. Tan, and J. Li, Appl. Opt. **44**, 2575 (2005).
19) K. Tanaka, M. Hara, K .Tokuyama, K. Hirooka, K. Ishikawa, A. Fukumoto, and

K. Watanabe, Opt. Express **15**, 16196 (2007).

20) C. E. Hoyle, T. Y. Lee, and T. Roper, J. Polym. Sci. A **42**, 5301 (2004).
21) L. V. Natarajan, C. K. Shepherd, D. M. Brandelik, R. L. Sutherland, S. Chandra, V. P. Tondiglia, D. Tomlin, and T. J. Bunning, Chem. Mater. **15**, 2477 (2003).
22) L. V. Natarajan, D. P. Brown, J. M. Wofford, V. P. Tondiglia, R. L. Sutherland, P. F. Lloyd, and T. J. Bunning, Polymer **47**, 4411 (2006).
23) E. Hata and Y. Tomita, Opt. Mater. Express **1**, 1113 (2011).
24) T. Kume, S. Yagi, T. Imai, and M. Yamamoto, Jpn. J. Appl. Phys. **40**, 1732 (2001).
25) J. A. Frantz, R. K. Kostuk, and D. A. Waldman, J. Opt. Soc. Am. A **21**, 378 (2004).
26) N. Suzuki and Y. Tomita, Appl. Opt. **46**, 6809 (2007).
27) R. M. Shelby, J. A. Hoffnagle, G. W. Burr, C. M. Jefferson, M.-P. Bernal, H. Coufal, R. K. Grygier, H. Günther, R. M. Macfarlane, and G. T. Sincerbox, Opt. Lett. **22**, 1509 (1997).
28) S. Yasuda, J. Minabe, and K. Kawano, Opt. Lett. **32**, 160 (2007).
29) Y.-W. Yu, C.-Y. Chen, C.-C. Sun, Opt. Lett. **35**, 1130 (2010).
30) J. Li, L. Cao, H. Gu, X. Tan, Q. He, and G. Jin, Opt. Lett. **37**, 936 (2012).